

Effects of Different Hydroxyapatite Binders on Morphology, Ca/P Ratio and Hardness of Nd:YAG Laser Clad Coatings

C. S. Chien¹, T. J. Han², T. F. Hong³, T. Y. Kuo^{2,*1} and T. Y. Liao^{2,*2}

¹Chimei Foundation Hospital, Tainan 710, Taiwan, R. O. China

²Department of Mechanical Engineering, Southern Taiwan University, Tainan 710, Taiwan, R. O. China

³Department of Materials Engineering, National Pingtung University of Science and Technology, Pingtung 912, Taiwan, R. O. China

Hydroxyapatite (HA) is a well known biocompatible coating material used to improve the bonding quality between metallic substrates and the surrounding bone tissue following implantation. In this study, HA is mixed with two different binders, namely water glass (WG) and polyvinyl alcohol (PVA), respectively, and is then clad on Ti-6Al-4V substrates using an Nd:YAG laser beam. The results show that for both binders, the weld surface width, penetration depth and heat affected zone decrease with an increasing travel speed. The PVA binder increases the number and severity of the cracks in the transition layer of the weld bead, whereas the WG binder increases the porosity. In each coating layer, the middle level has the lowest Ca/P ratio, while the lower level has the highest value. Moreover, the Ca/P ratio reduces with an increasing travel speed. The microstructure of the transition layers is mainly composed of CaTiO₃, Ca₂P₂O₇, TiP₂, Ti, and HA phases. SiO₂ and Si₂Ti are additional phases found in the specimen used WG as binder material. The WG binder yields a higher hardness of the coating layer and transition layer than the PVA binder. However, for both binders, the hardness of the transition layer is generally far higher than that of the substrate or the coating layer. [doi:10.2320/matertrans.M2009245]

(Received July 14, 2009; Accepted September 11, 2009; Published November 25, 2009)

Keywords: Nd:YAG laser, polyvinyl alcohol, water glass, hydroxyapatite, clad

1. Introduction

In general, biomaterials can be classified as either biotolerated, bioinert, bioactive or bioabsorbable, depending on the response of the host tissue following implantation. Of all the bioactive ceramic materials currently available, hydroxyapatite (HA) and bioglass (BG) are amongst the most commonly used. However, due to their brittle nature, neither HA nor BG can be used alone for applications characterized by heavy stress cycles, such as artificial joints. By contrast, titanium (Ti) and its alloys are ideally suited for medical implants due to their lightness, high strength/elastic modulus ratio, excellent corrosion resistance and good biocompatibility. However, such metals are bioinert, and therefore do not easily form chemical bonds with the host tissue. As a result, Ti-based implants tend to become detached from the host tissue following long-term implantation. Furthermore, eroded or partially worn metallic implant surfaces release harmful metallic ions into the human body.¹⁻³ In practice, both problems can be resolved to a large extent by coating the metallic implant with a thin layer of bioactive material such as HA or BG.

The bonding quality between the Ti substrate and the bioactive coating is dependent upon the coating method. In investigating the adhesive and bioactivity properties of HA and BG coatings, most previous studies have considered plasma spraying,⁴⁻⁶ pulsed laser deposition (PLD),⁷⁻⁹ or sol-gel coating¹⁰⁻¹² techniques. However, these methods generate a mechanical rather than metallurgical bonding between the coating and the substrate, and hence the bonding strength is relatively low. In addition, the adhesive performance of such coatings deteriorates significantly following soaking in

simulated body fluid (SBF).¹³ Finally, the coating tends to crack during the deposition process due to the large mismatch in the thermal expansion coefficients of the coating and the Ti substrate, i.e. $13.3 \times 10^{-6} \text{ K}^{-1}$ and $\sim 8.4-8.8 \times 10^{-6} \text{ K}^{-1}$, respectively.

Recent studies have shown that the use of a laser cladding technique results in a metallurgical bonding between HA coatings and Ti-6Al-4V substrates.¹⁴⁻¹⁹ Laser cladding is generally performed using either a CO₂ laser or an Nd:YAG laser. Of the two lasers, the Nd:YAG laser has a better absorption efficiency, and is therefore preferred in this study. In Ref. 15) and 19), the HA powder was mixed with water glass (WG) and polyvinyl alcohol (PVA), respectively, prior to the cladding process in order to obtain a paste state. In the present study, HA powder samples are prepared using either WG or PVA additives, respectively, such that the effects of the two different binders can be evaluated and compared. The powder samples are then clad on Ti-6Al-4V substrates using an Nd:YAG laser beam. A series of experiments are then performed to investigate the effects of the binder, the laser travel speed, and the laser output power on the morphology, Ca/P ratio and hardness of the various coatings.

2. Experimental Procedure

The Hydroxyapatite (HA, Ca₁₀(PO₄)₆(OH)₂) powders used in the present study was supplied by Showa Inc., Japan. HA was mixed with a binder material (either PVA((C₂H₄O)_n) or WG (Na₂O·nSiO₂)) by 50 : 50 in mass% and then well stirred into slurry. The chemical composition of the Ti-6Al-4V alloy used in the present experiments is shown in Table 1. Substrates for the laser cladding process were prepared by machining the Ti alloy into thin plates with dimensions of 100 mm × 60 mm × 3.8 mm. The size and

*1Corresponding author, E-mail: tykuo@mail.stut.edu.tw

*2Graduate Student, Southern Taiwan University

Table 1 Chemical composition (mass%) of Ti-6Al-4V.

	Al	V	O	Fe	C	N	H	Ti
Ti-6Al-4V	6.1	4.24	0.152	0.16	0.017	0.008	0.0006	Bal.

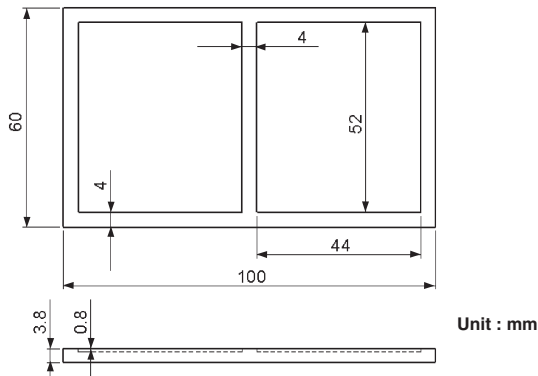


Fig. 1 Schematic diagrams of specimen design.

Table 2 Parameters used in Nd:YAG laser cladding process.

Power (W)	Travel Speed (mm/min)	Laser Incident Angle (°)	Defocus Length (mm)	Shielding Gas	Pre-plate Thickness (mm)
740	200, 300, 400	5	15	Ar	0.8
1150	300, 400, 500				

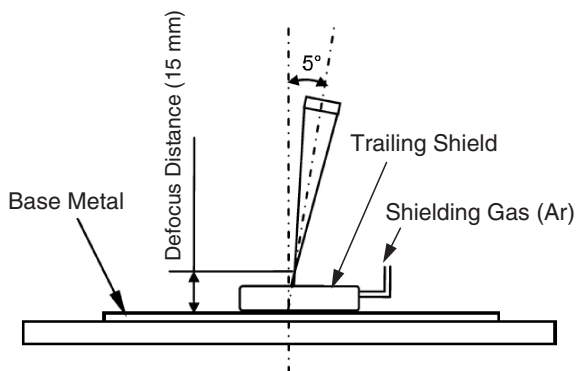


Fig. 2 Experimental setup for Nd-YAG laser cladding process.

shape of the specimen used in the study are schematically shown in Fig. 1. Two slots (52 mm × 44 mm × 0.8 mm) were milled on the Ti-6Al-4V plate, refilled with the HA+binder slurry, and then leveled the slurry by a stainless steel scraper. Following a drying process, the samples were laser clad using an Nd-YAG laser set to a continuous wave (CW) mode under two different output powers and three different travel speeds. The laser cladding experiments were conducted in an Ar shielded atmosphere (Ar flow rate: 25 l/min) using a 5° incident angle and a 15 mm defocus length. The experimental parameters and setup are shown in Table 2 and Fig. 2, respectively. The microstructures of the clad specimens were characterized via optical microscopy (OM) and scanning electron microscopy (SEM). The Ca/P

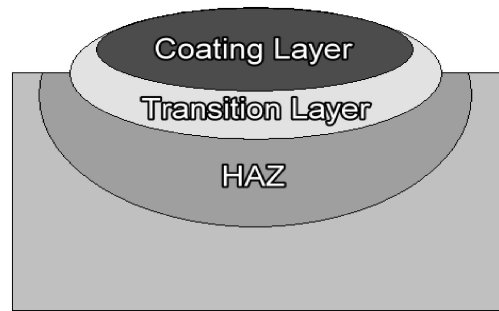


Fig. 3 Schematic diagram showing three zones in weldment (cross-section).

ratio of the coating layer was calculated from the atomic percentage of Ca and P in the structure measured by energy dispersive X-ray spectrometer (EDS) equipped in SEM. The phases of transition layer were analyzed by X-Ray diffraction (XRD). Finally, the adhesive strength of the various coatings was estimated qualitatively from the cracks formed in the interface between the coating layer and transition layer during indentation by the diamond pyramid tip of a Vickers hardness tester.

3. Results and Discussion

3.1 Morphology and microstructure of weld beads

As shown in Fig. 3, the cross-section of the weld bead comprises three distinct regions, namely the coating layer, the transition layer and the heat affected zone (HAZ). Figure 4 presents OM images of the weld surfaces and weld bead profiles (cross-section) produced using different binders, laser powers and travel speeds. The results clearly show that for both binders, the weld bead has a shallow bowl-shaped (∩) profile when the cladding process is performed using a 740 W laser power, but has an inverted bell-shaped (∪) profile when the laser power is increased to 1150 W. In addition, it is observed that the surface width, penetration depth, and HAZ all decrease with an increasing travel speed due to the corresponding reduction in the average heat input.

The temperature derived from the laser beam on the cladding surfaces cannot be measured accurately because laser cladding is a process of rapidly heating and cooling.^{20,21)} However, the temperature field of the laser cladding process (substrate: Ti-6Al-4V, cladding material: HA) was simulated by means of finite element analysis method.²²⁾ The result shows that the maximum temperature has reached 1919°C and it is higher than the melting point of the cladding and substrate materials. The cracks and pores formed in the structure were highly affected by the high temperature derived from the laser beam and the rapid heating and cooling process.

Comparing the two sets of images presented in Fig. 4, it can be seen that the use of a PVA binder increases the number and severity of the cracks in the transition layer, whereas the WG binder increases the porosity of the transition layer (see also Fig. 5). The difference in porosity of the PVA and WG specimens is most likely the result of the difference in the melting temperatures of the two binders, i.e. 1300°C for

Power (W)	Travel Speed (mm/min)	PVA		WG	
		Weld Surface	Weld Bead Profile	Weld Surface	Weld Bead Profile
740	200				
	300				
	400				
1150	300				
	400				
	500				

Fig. 4 Weld surfaces and bead profiles (cross-section) for various laser powers and travel speeds.

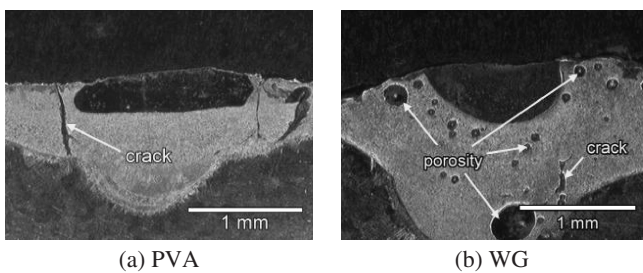


Fig. 5 Weld defects in transition layer of weld beads produced using different binders. (a) PVA (1150W, 300mm/min); (b) WG (1150W, 300mm/min)

WG and 240°C for PVA. Due to the relatively low melting temperature of the PVA binder, the PVA content in the HA powder is vaporized and released completely into the surrounding atmosphere during the initial stages of the laser cladding process. However, the melting temperature of WG is close to that of HA (1650°C) and Ti-6Al-4V (1670°C). Since the HA and Ti-6Al-4V solidify rapidly during the cladding process, the vaporized WG becomes trapped within the molten metal and forms pores within the weld bead as it cools.

Observing the weld bead profiles in Figs. 4 and 5, it is noted that the samples prepared using WG as the binder

material have a more raised surface than those prepared using PVA. This is thought to be the result of the Si and O contents in WG, which collectively create a positive surface tension coefficient in the fusion zone²³⁾ and therefore prompt an inward surface flow of the molten metal toward the central region of the weld bead.

3.2 Ca/P ratio of coating layers

HA has a Ca/P ratio of 1.67. However, the Ca/P ratio of the current HA-based coatings depends on both the choice of binding powder and the welding parameters used in the cladding process. Figure 6 summarizes the Ca/P ratios of the upper, middle and lower levels of the various HA/PVA and HA/WG coatings. Overall, it is observed that the Ca/P ratios of the coating layer after heating by the laser beam are higher than that of HA, while the lower level has the highest value, and the WG samples have a relatively higher Ca/P ratio than their PVA counterparts. It is revealed that P was partly dissipated from the structure after heating at the high temperature. Also, when the binder was vaporized from the molten pool, it stimulated the agitation of the molten pool and hence helped the P dissipation. Nevertheless, the increase of laser travel speed has a trend of reducing the P dissipation.

In this study, although HA was melted with the binder and the Ca/P ratio was highly raised due to P was vaporized

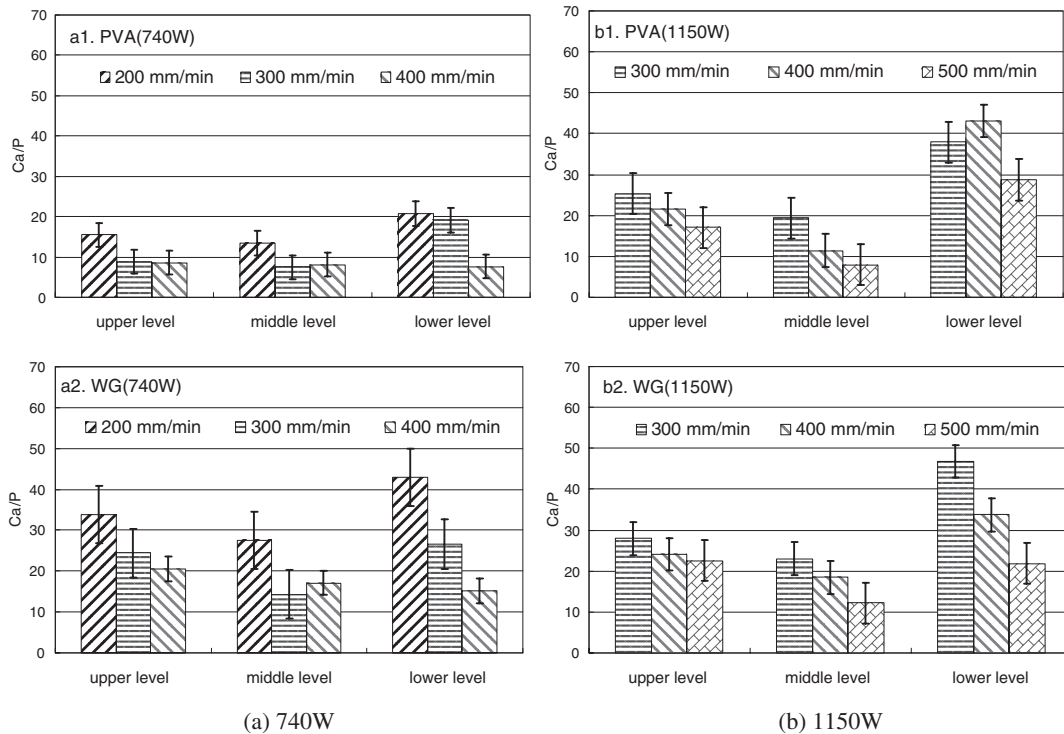


Fig. 6 Comparison of Ca/P ratios of upper, middle and lower levels in coating layer for various laser powers and travel speeds.

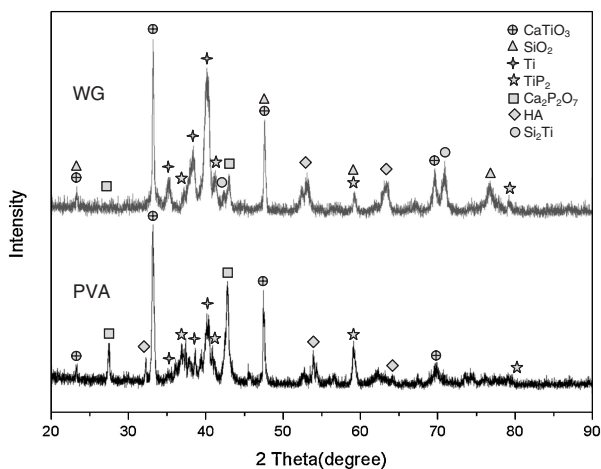


Fig. 7 XRD analysis of the transition layer of the specimen using different binders.

during the process. However, Chao²⁴⁾ recently reported that after cladding HA on Ti-6Al-4V substrates using an Nd:YAG laser beam, a layer of bone-like apatite could be effectively formed after immersing in a simulated body fluid (SBF). It reveals the sample has sufficient bioactivity to form chemical bonds with the host tissue.

3.3 The composition analysis

Figure 7 shows the XRD spectrum of the transition layers. It reveals that the transition layer is mainly composed of CaTiO_3 , $\text{Ca}_2\text{P}_2\text{O}_7$, TiP_2 , Ti and HA. $\text{Ca}_2\text{P}_2\text{O}_7$ was produced from the decomposition of HA at high temperature, whereas CaTiO_3 and TiP_2 were produced by reacting with the substrate materials after the decomposition of HA.^{14-16,25)}

Moreover, it is also observed that the transition layer of the sample using WG binder would additionally include of SiO_2 and Si_2Ti phases. This result indicates that most WG binder became slag and floated to the weld surface during the laser cladding process. On the contrary, PVA was vaporized and released into surrounding atmosphere completely at the initial laser cladding stage so that there was no other contaminated production left in the structure.

3.4 Hardness evaluation

Figure 8 presents the Vickers hardness profiles of the various weld beads from the central coating layer (CL), across the transition layer (TL), and into the Ti alloy substrate. It can be seen that in the majority of cases, the transition layer has a far higher hardness than either the substrate or the coating layer. When performing the cladding process using a WG binder and a welding power and travel speed of 740 W and 400 mm/min, respectively, both the coating layer and the transition layer are very thin, and thus their hardness values are very similar to those of the substrate. In addition, for both binders, the width and average hardness of the transition layer increase with an increasing laser power or a decreasing travel speed.

The published literature contains very little information regarding the effect of the hardness of the transition layer on the coating quality. The transition layers in the weld beads formed in this study have a hardness of at least 1000 HV. As shown in Fig. 9, a micro crack is formed within the transition layer following indentation using a pyramid tip. However, in Fig. 10, no cracks are observed in any of the samples when the indentation test is performed at the interface between the coating layer and the transition layer, which exhibits a satisfied adhesion in between. From the

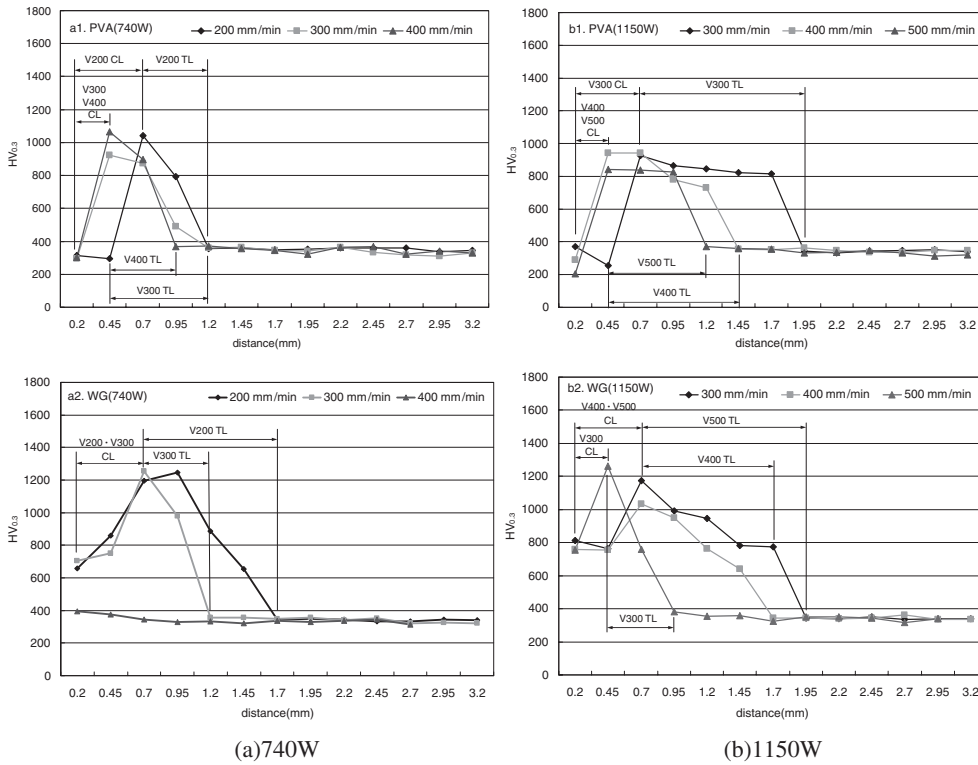


Fig. 8 Vickers hardness profiles of weld beads from central coating layer, to transition layer, to substrate for various laser powers and travel speeds. (Note V: welding speed; CL: coating layer; TL: transition layer.)

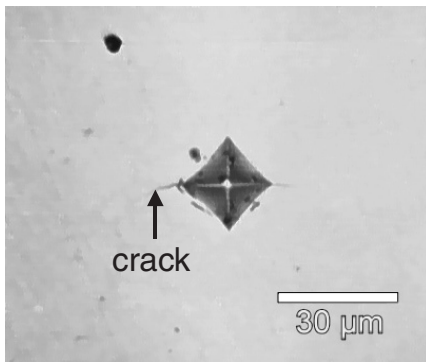


Fig. 9 Vickers indentation mark in transition layer.

microhardness distribution analysis in Fig. 8, although the transition layer has a high hardness, it can be seen that the microhardness revealed a gradual change from the transition layer to substrate and there was no obvious demarcation near the interface. This indicates that the mechanical properties should not be serious degraded. Zheng *et al.*²⁶ also reported that such gradual decreased microhardness could help stress relaxation between coating and host tissue after following implantation.

4. Conclusion

This study has performed a systematic investigation into the effects of the HA binder (i.e. PVA or WG), the laser output power and the travel speed on the morphology, Ca/P ratio and hardness of Nd-YAG laser clad coatings on a

Ti-6Al-4V substrate. The experimental results support the following major conclusions:

- (1) The weld beads formed using a relatively low laser power of 740 W have a shallow bowl-shaped (☪) profile, while those formed using a high laser power of 1150 W have an inverted bell-shaped (☽) profile. For both binders, the weld surface width, penetration depth, and heat affected zone all reduce with an increasing laser travel speed. In addition, the PVA binder increases the number and severity of the cracks formed in the transition layer of the weld bead, whereas the WG binder increases the porosity of the transition layer.
- (2) For both the PVA and the WG binders, the middle level in the coating layer has the lowest Ca/P ratio while the lower level has the highest value. In general, the Ca/P ratio decreases with an increasing travel speed, but increases with an increasing laser output power.
- (3) The transition layer of all specimen is mainly composed of CaTiO₃, Ca₂P₂O₇, TiP₃, Ti, and HA phases. SiO₂ and Si₂Ti are additional phases found in the specimen used WG as binder material.
- (4) The coating layer and transition layer of the samples prepared using the WG binder have a higher hardness than the equivalent layers in the samples prepared using PVA binder. In addition, in the majority cases, the transition layer is significantly harder than the substrate or the coating layer. The width and average hardness of the transition layer increase with an increasing laser power or a reducing travel speed.

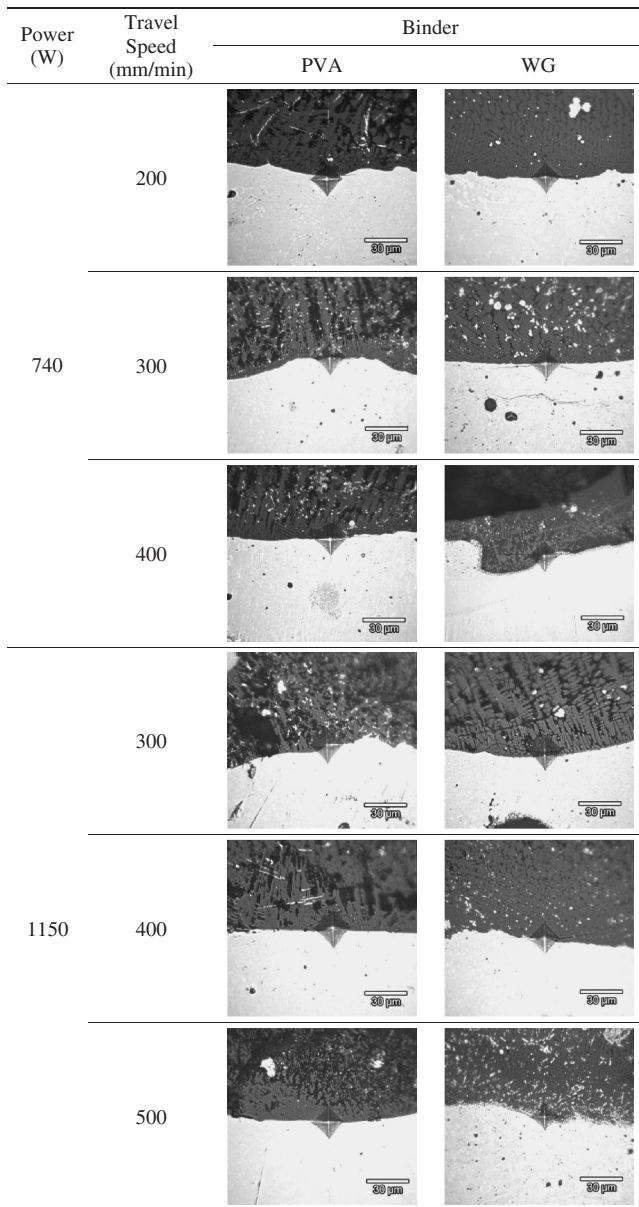


Fig. 10 OM images of interface between coating layer (dark) and transition layer (white) following HV hardness tests in weld beads produced using various laser powers and travel speeds.

REFERENCES

- 1) S. Itoh, T. Muneta, K. Shinomiya and S. Ichinose: *J. Mater. Sci. Mater. Med.* **8** (1999) 185–190.
- 2) H. Tomas, G. S. Cavalho, M. H. Fernandes, A. P. Freire and L. M. Abrantes: *J. Mater. Sci. Mater. Med.* **7** (1996) 291–296.
- 3) H. S. Dobbs and M. J. Minski: *Biomaterials* **1** (1980) 193–198.
- 4) E. Chang, W. J. Chang, B. C. Wang and C. Y. Yang: *J. Mater. Sci. Mater. Med.* **8** (1997) 193–200.
- 5) K. A. Khor, P. Cheang and Y. Wang: *J. Therm. Spray Techn.* **7** (1998) 254–260.
- 6) P. L. Silva, J. D. Santos, F. J. Monteiro and J. C. Knowles: *Surf. Coat. Tech.* **102** (1998) 191–196.
- 7) O. Blind, L. H. Klein, B. Dailey and L. Jordan: *Dent. Mater.* **21** (2005) 1017–1024.
- 8) V. Nelea, V. Craciun, M. Iliescu, I. N. Mihailescu, H. Pelletier, P. Mille and J. Werckmann: *Appl. Surf. Sci.* **208–209** (2003) 638–644.
- 9) G. Socol, P. Torricelli, B. Bracci, M. Iliescu, F. Miroiu, A. Bigi, J. Werckmann and I. N. Mihailescu: *Biomaterials* **25** (2004) 2539–2545.
- 10) W. Weng and J. L. Baptista: *J. Am. Ceram. Soc.* **82** (1999) 27–32.
- 11) E. Milella, F. Cosentino, A. Licciulli and C. Massaro: *Biomaterials* **22** (2001) 1425–1431.
- 12) H. W. Kim, Y. H. Koh, L. H. Li, S. Lee and H. E. Kim: *Biomaterials* **25** (2004) 2533–2538.
- 13) S. W. K. Kweh, K. A. Khor and P. Cheang: *Biomaterials* **23** (2002) 775–785.
- 14) Y. Sen and C. M. Hau: *Key Eng. Mater.* **330–332** (2007) 569–572.
- 15) C. Z. Chen, D. G. Wang, P. Xu, Q. H. Bao, L. Zhang and T. Q. Lei: *Chin. J. Lasers* **31** (2004) 1021–1024 (in Chinese).
- 16) Y. Wang, J. C. Gao and Y. P. Zhang: *Chin. J. Lasers* **31** (2004) 487–490 (in Chinese).
- 17) D. G. Wang, C. Z. Chen, J. Ma and T. Q. Lei: *Appl. Surf. Sci.* **253** (2007) 4016–4020.
- 18) G. J. Cheng, D. Pirzada, M. Cai, P. Mohanty and A. Bandyopadhyay: *Mater. Sci. Eng. C* **25** (2005) 541–547.
- 19) D. Chi and Y. Wang: *Surf. Tech.* **35** (2006) 31–37 (in Chinese).
- 20) W. D. Zhu and Q. B. Liu: *Laser Technol.* **26** (2002) 183–185.
- 21) J. L. Liu and Z. R. Zou: *Heat treatment with high energy beam*, Beijing, (Machinery Industry Press, 1997).
- 22) W. D. Zhu, Q. B. Liu, H. T. Li and M. Zheng: *Mater. Design* **28** (2007) 2637–267.
- 23) S. B. Lin, C. L. Yang, F. Y. Liu, L. Wu and S. Su: *Weld. Res. Abroad* **48** (2002) 46–50.
- 24) C. L. Chiao: Master Thesis, (Southern Taiwan University, Tainan, Taiwan, 2009).
- 25) Z. Haitong and R. L. William: *Biomaterials* **21** (2000) 23–30.
- 26) M. Zheng, D. Fan, X. K. Li, W. F. Li, Q. B. Liu and J. B. Zhang: *Appl. Surf. Sci.* **255** (2008) 426–428.